Electric Transport Properties of Surface-Anchored Metal–Organic Frameworks and the Effect of Ferrocene Loading

ARTICLE *in* ACS APPLIED MATERIALS & INTERFACES · APRIL 2015

Impact Factor: 6.72 · DOI: 10.1021/acsami.5b01792 · Source: PubMed

ACS APPLIED MATERIALS & INTERFACES

Research Article

www.acsami.org

Electric Transport Properties of Surface-Anchored Metal–Organic Frameworks and the Effect of Ferrocene Loading

Jianxi Liu,[†] Tobias Wächter,[‡] Andreas Irmler,[§] Peter G. Weidler,[†] Hartmut Gliemann,[†] Fabian Pauly,[§] Veronica Mugnaini,*[,†] Michael Zharnikov,[‡] and Christof Wöll*[,†]

[†]Institute of Functional Interfaces (IFG), Karlsruhe Institute of Technology (KIT), 76344 Eggenstein-Leopoldshafen, Germany

[‡]Applied Physical Chemistry, University of Heidelberg, 69120 Heidelberg, Germany

[§]Department of Physics, University of Konstanz, 78457 Konstanz, Germany

Supporting Information

ABSTRACT: Understanding of the electric transport through surface-anchored metal–organic frameworks (SURMOFs) is important both from a fundamental perspective as well as with regards to possible future applications in electronic devices. To address this mostly unexplored subject, we integrated a series of representative SURMOF thin films, formed by copper nodes and trimesic acid and known as HKUST-1, in a mercury-drop-based tunneling junction. Although the transport properties of these SURMOFs are analogous to those of hybrid metal–organic molecular wires, manifested by a very low value of the tunneling decay constant ($\beta \approx 0.006$ Å^{-1}), they are at the same time found to be consistent with a linear increase of resistance with film thickness. Upon loading of SURMOF pores with ferrocene (Fc), a noticeable increase in transport current was observed. A transport model and ab initio electronic structure calculations were used to reveal a hopping transport mechanism and to relate the changes upon Fc loading to those of the electronic and vibrational structures of the SURMOF films.

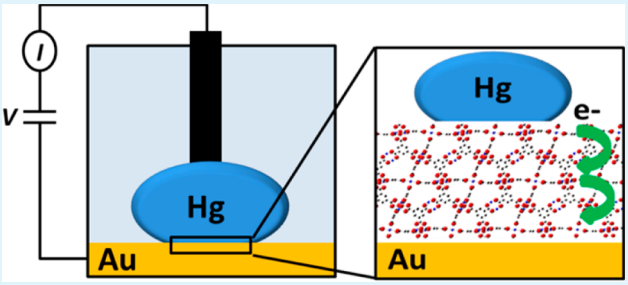

KEYWORDS: *surface-anchored metal–organic frameworks, electric transport properties, conduction mechanism, mercury-based tunneling junctions, density functional theory*

1. INTRODUCTION

Metal–organic frameworks (MOFs)[1−5] are coordination polymers formed by metal nodes or clusters connected by organic ligands to give crystalline three-dimensional networks with well-defined pores. Thanks to their porosity, MOFs have been largely investigated as potentially suitable host architectures for a variety of different applications, ranging from storage[6−8] to delivery,[9] sensing,[10] and catalysis,[11] to name a few. Additionally, recently, MOFs have been considered as possible components of electronic devices[12−16] with either an active electronic role, i.e., being involved in the charge transport, or a mere supplementary role, as porous scaffolds in batteries,[17,18] fuel cells,[19] and capacitors.[20] Even though the foreseen potential of MOFs for electronic applications is very promising, the investigation of their fundamental transport properties is still in its incipiency. To address this issue, we integrated a MOF formed by copper nodes and trimesic acid, and known as HKUST-1,[21] in a mercury-drop-based tunneling junction. The HKUST-1 was prepared as highly oriented crystalline film with adjustable thickness on a carboxylic terminated self-assembled monolayer (SAM) on gold by means of the stepwise liquid phase epitaxy method.[22,23] The obtained surface-anchored MOF (SURMOF) films of high quality, compactness, and low defect density[24] were used as bottom electrode in a Hg-based tunneling junction,[25−28] where the liquid Hg drop is the top electrode (see Figure 1), and their charge-transport properties were investigated.

2. EXPERIMENTAL SECTION

Materials. Copper acetate monohydrate (Cu^{2+}), 1,3,5-benzenetricarboxylic acid (BTC), ferrocene (Fc), hexadecane (HD), and hexadecanethiol (HDT, Figure 1, right) were obtained from Sigma-Aldrich and used without any further purification. Ethanol was purchased from VWR. The 9-carboxy-10-(mercaptomethyl)triptycene thiol (CMMT, Figure 1, right) was prepared according to literature.[29] The gold substrates were obtained from Georg Albert PVD (Silz, Germany). They were prepared by thermal evaporation of 100 nm of gold (99.99% purity) onto polished single-crystal silicon (100) wafers (Silicon Sense) using a 5 nm titanium adhesion layer. The evaporated films were polycrystalline, with grains having predominantly a [111] orientation. The as-deposited Au substrates were kept in Ar filled containers until use.

General Preparation Procedure. *SAM Preparation.* Gold substrates were immersed into an ethanolic solution of 9-carboxy-10-(mercaptomethyl) triptycene (CMMT; 20 μM) for 72 h at room temperature in the dark. Thereafter, the substrates were rinsed with

Received: February 27, 2015
Accepted: April 15, 2015
Published: April 15, 2015

DOI: 10.1021/acsami.5b01792
ACS Appl. Mater. Interfaces 2015, 7, 9824−9830

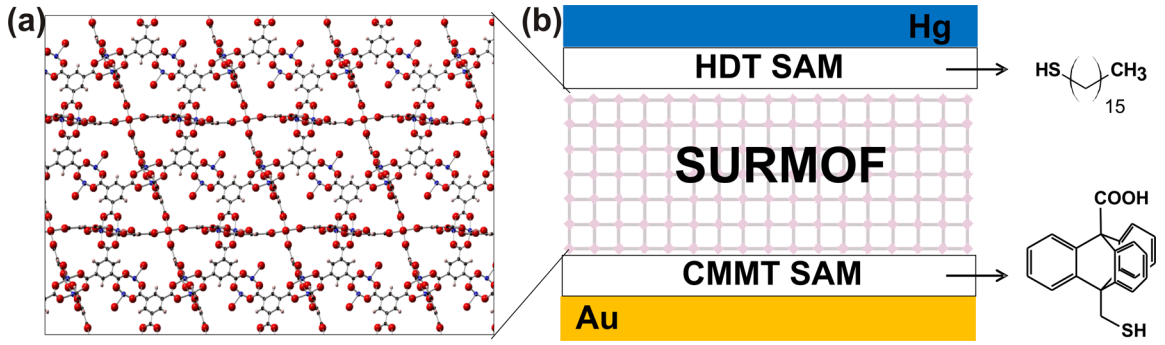

Figure 1. Scheme of the Hg-based tunneling junction. (a) Crystal structure of HKUST-1 with [111] orientation with respect to the gold surface. Oxygen, carbon, and copper atoms are coded in red, blue, and black colors, respectively. (b) Contact area between the two electrodes: Hg as top electrode is passivated with a SAM of hexadecanethiol ($C_{16}H_{33}$–SH, HDT), whereas the SURMOF grown on a 9-carboxy-10-(mercaptomethyl) triptycene (CMMT) modified Au substrate serves as bottom electrode. The molecular formulas of HDT and CMMT are presented on the right side.

ethanol and dried with a N_2 stream. This procedure was performed shortly before SURMOF preparation; a schematic representation of the CMMT SAM is shown in Figure 1 and Figure S1 in the Supporting Information.

SURMOF Preparation. The liquid phase epitaxy (LPE) grown HKUST-1 SURMOFs with different thickness were prepared on CMMT modified Au substrates by the spray method according to the procedure reported in the literature[30] and schematized in Figure S2 in the Supporting Information. Copper acetate (1 mM in ethanol) and 1,3,5-benzenetricarboxylic acid (0.1 mM in ethanol) were alternately sprayed on the target CMMT SAM for 15 and 20 s, respectively. After the spraying of each component, we waited for 25 s and then the target was abundantly rinsed with ethanol to remove any unselectively bound material. The spraying of the metal and linker solutions (i.e., a cycle) was then repeated 5, 7, or 10 times. The crystal structure of the HKUST-1 SURMOF is shown in Figure 1a.

SURMOF Loading. To get rid of residual solvent molecules trapped inside the pores and to achieve an efficient loading, the pristine HKUST-1 SURMOF samples were placed in a Petri dish and heated to 60 °C in air for 20 min.[24] Thereafter, the samples were exposed to a vapor of ferrocene at room temperature for 72 h.

Methods. *X-ray Diffraction (XRD).* Out-of-plane XRD was carried out on a Bruker D8 Advance in θ–θ geometry equipped with a Si-strip detector (PSD Lynxeye©) using Cu K$\alpha_{1,2}$ radiation. On the tube side a variable divergence slit set to V12 (variable slit opening with 12 mm sample spot size) and on the receiving side a 2.5° Soller slit were used. Scans ran from 5 to 20° (2θ) with a step width of 0.024° and 16.4 s per step. To compare the measured intensity for different spray cycles, the same sample was used for each XRD measurement, providing the same irradiated area.

Infrared Reflection Absorption (IRRA) Spectroscopy. The IRRA spectra of the HKUST-1 SURMOFs before and after ferrocene loading were acquired using the infrared spectrometer Bruker VERTEX 80v. The absorption band positions are given in wave numbers ν in cm^{-1}, with a resolution of 2 cm^{-1}. All the IRRA spectra were recorded in grazing incidence reflection mode at an angle of incidence amounting to 80° relative to the surface normal using liquid nitrogen cooled mercury cadmium telluride (MCT) narrow band detectors. Perdeuterated hexadecanethiol SAMs on Au/Si were used for background measurements.

Atomic Force Microscopy (AFM). AFM measurements were performed on a Multimode (Bruker) with a "J" scanner at a scan speed of 0.4 Hz under ambient laboratory conditions of 21–24 °C. Film thicknesses of the SURMOFs were obtained in tapping mode, and the cantilever type was a Mikromasch HQ: NSC18. Scan sizes were of 60 μm^2.

Assembly of Hg-Based Junctions. The home-built mercury-drop setup described by Zharnikov et al. was used.[31] A mercury drop (around 600 μm in diameter) was extruded from a gastight Hamilton syringe, whose plunger metallic core is connected to a Keithley 2635A source meter through a tungsten wire. The HKUST-1 SURMOF samples, used as bottom electrodes, were also put in contact with the source meter by means of a metal clip and a suitable cable connector. Right before the measurements, the mercury drop was prepared according to the standard protocol by immersion in 10 mM hexadecanethiol (HDT) solution in hexadecane for around 15 min. The HDT passivated mercury drop was then gently positioned on top of the SURMOF HKUST-1 samples. The deposited drop was observed with a CMOS camera with a Macro lens (The Imaging Source DMK22AUC03 1/3 in. Micron with MR 8/O). From the sideway view of the junction, the diameter of drop was measured and hence the contact area value calculated. One mM HDT solution in hexadecane was used to increase the stability of the drop and avoid amalgamation.[32] The whole setup was placed on a vibration isolation table and put inside a home-built Faraday cage to reduce vibrations and electrical noise, respectively. For each system, 3 different samples were used with 5 different positions for each sample. For each position, 4–6 current–voltage curves were recorded. All the recorded current–voltage curves were used, unless they showed conductance values resembling a metal–metal contact and hence came from rupture or amalgamation of the Hg-drop. In the plots, the average extracted from all the recorded curves has been plotted. Data points were collected using a voltage ramp with a step size of 49 mV (between 0.01 and 0.5 V) and a time interval of at least 5 s between individual steps.

Theoretical Analysis of Charge Transport Mechanism. To understand the charge transport in SURMOFs, we have studied a one-dimensional toy model that describes the transition from tunneling to hopping conduction.[33] It takes dephasing into account by connecting each chain site to an external, phase-randomizing reservoir. In addition to gain insight into the electronic structure of HKUST-1, we performed DFT calculations with the program package TURBOMOLE.[34] We used the def-TZVP basis set and the B3-LYP hybrid functional with empirical dispersion corrections.[35,36] It has been shown that this exchange-correlation functional leads to a good description of the fragments of the HKUST-1 MOF.[37]

3. RESULTS AND DISCUSSION

The SURMOF HKUST-1 thin films were prepared on the SAM formed by 9-carboxy-10-(mercaptomethyl) triptycene, CMMT,[29] by means of the sequential step-by-step spray method,[30] as described in the Supporting Information. Films of different thickness were obtained by varying the number of spraying cycles (5, 7, and 10). All the films were characterized in detail by IRRA spectroscopy and out-of-plane XRD. In all cases, the films had the expected crystalline [111] orientation (Figure 2a, black), as shown by the presence of the characteristic (111), (222) and (333) Bragg peaks (with 2θ of 5.84, 11.67, and 17.54°, respectively).

DOI: 10.1021/acsami.5b01792
ACS Appl. Mater. Interfaces 2015, 7, 9824–9830

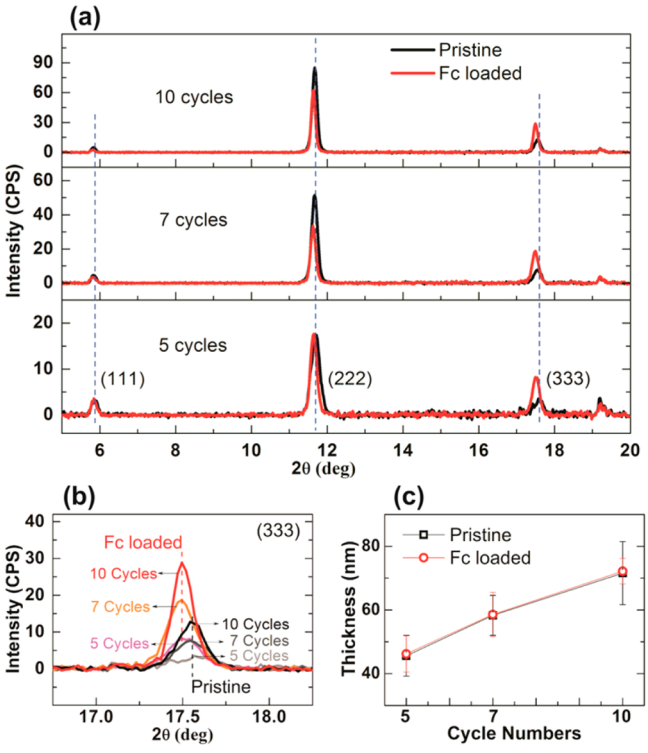

Figure 2. (a) Out-of-plane XRD of the pristine (black) and ferrocene-loaded (red) HKUST-1 SURMOF samples. From top to bottom: 10, 7, and 5 spraying cycles. (b) Zoom in on the (333) Bragg peak to monitor the shift to lower 2θ values after the ferrocene loading. (c) Dependence of the SURMOF thickness, as measured by AFM, on the number of spraying cycles for both pristine HKUST-1 SURMOFs (black empty squares) and after ferrocene loading (red empty circles).

The intensity of the recorded reflexes, which can be correlated with the size of the coherent scattering domains, increases with the SURMOF thickness, suggesting that the vertical dimensions of the ordered domains are noticeably larger.[30] The film thickness has been measured by atomic force microscopy (AFM) and was found to be 45.6 ± 6.4, 58.3 ± 6.3, and 71.6 ± 9.9 nm for the 5, 7, and 10 spraying cycles, respectively. IRRA spectra, evaluation of XRD data and AFM images are reported in the Supporting Information, Figures S3−S7.

The tunneling junction was assembled as reported in the literature,[31] viz. a drop of Hg was passivated with hexadecanethiol ($C_{16}H_{33}$−SH, HDT) to avoid amalgamation and short-cuts and then gently contacted to the bottom electrode in a cell filled with HDT in hexadecane. The stability of the HKUST-1 SURMOF over time under these experimental conditions was proved by out-of-plane XRD (Figure S8 in the Supporting Information). Before investigating the SURMOF films, the reliability of the setup was checked by using the CMMT SAM on Au as the bottom electrode. The current flowing through the Hg/HDT//CMMT/Au junction was measured while sweeping the bias voltage (V) in the negative (−0.5 V to −0.01 V) and positive range (0.01−0.5 V). Evaluation of the contact area by observation of the extruded Hg drop with an optical microscope enabled us to calculate the current density J under the applied voltage V. The semilog plot of the current density vs voltage for the CMMT SAM is shown in Figure 3a in green. The measured values are in good agreement with those reported for SAMs of comparable thickness,[31] marked for the sake of comparison in Figure 3a as a blue star.

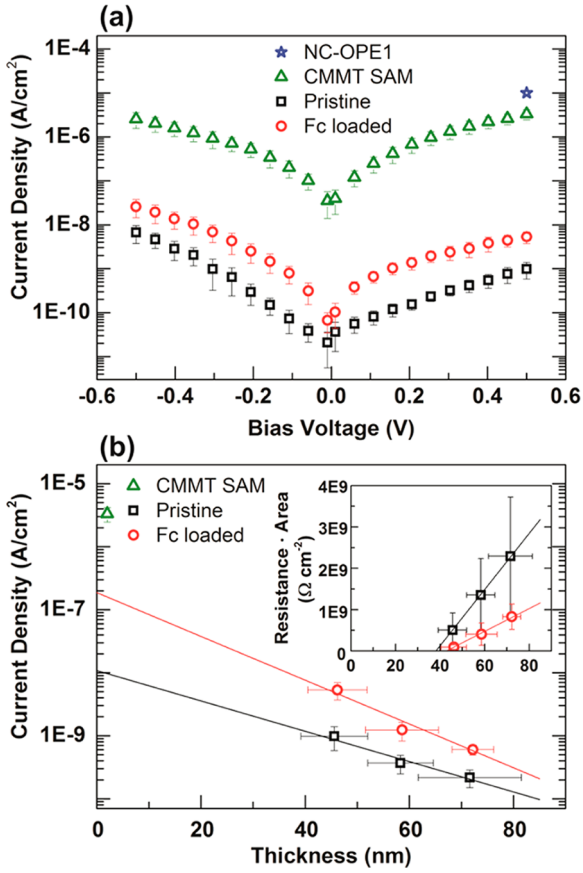

Figure 3. (a) Log J vs V plot for HKUST-1 SURMOF, prepared by 5 spraying cycles, before (black empty squares) and after (red empty circles) the loading with ferrocene. Green empty triangles correspond to the CMMT SAM. The blue star represents the current density at a bias voltage of 0.5 V for a nitrile-substituted phenylthiol (NC-OPE1) SAM,[31] which has a comparable thickness to the CMMT SAM and is given for comparison. (b) Logarithm of current density at 0.5 V vs thickness of HKUST-1 SURMOFs, pristine (black empty squares) and after ferrocene loading (red empty circles). From the slope, the decay factor β has been calculated. A green triangle marks the current density for the CMMT SAM. The inset displays resistance times area vs thickness of HKUST-1 SURMOFs, pristine (empty black squares) and after ferrocene loading (empty red circles). The data is obtained as V/J at V = 0.5 V. Straight lines show linear fits, corresponding to an ohmic, linear increase in resistance with length.

Thereafter, the HKUST-1 SURMOF films were assembled in the junctions of the type Hg/HDT//HKUST-1/CMMT/Au. The semilog plot of the current density J vs V for the thinnest film (5 cycles) is shown in Figure 3a in black, whereas the analogous plots for the 7 and 10 spraying cycles samples are reported in Figure S9 in the Supporting Information. As can be clearly seen, the values of J for all the HKUST-1 SURMOF films are by far lower (by at least 2 orders of magnitude) than those of the CMMT SAM. This result confirms that the prepared SURMOF films, separating the Hg and Au electrodes by a distance of up to about 70 nm, are compact, of high quality, and with no major defects that would otherwise cause short-cuts.[24] The measured low conductance reflects also the poor intrinsic conductivity of HKUST-1, in agreement with what was already reported for non-oriented films of HKUST-1

DOI: 10.1021/acsami.5b01792
ACS Appl. Mater. Interfaces 2015, 7, 9824−9830

(around 1×10^{-6} S m^{-1}).[38] Additionally, the prepared films appear robust, as tested by varying the pressure applied through the drop on the SURMOF (Figure S10 in the Supporting Information). Very favorable mechanical properties of monolithic SURMOF thin films have also been reported in previous work based on the results of indentation experiments.[39]

The used setup, with a Hg drop as top electrode gently pressed against the SURMOF, combined with the possibility to prepare films of known and adjustable thickness, allow us to gain insight into the charge transport mechanism in MOFs by correlating the measured conductance G per area A (or the measured current density $J = GV/A$ at a fixed voltage) to the thickness of the investigated film. Indeed, analogously to what is generally done for metal-molecule-metal junctions, we can extract from our experimental data the slope β of a linear fit of the semilog plot of J at a specific voltage value vs film thickness.[25−28,31,40] This slope is also called "tunneling decay constant" or "attenuation factor". We will use these terms here for reasons of compatibility with the literature, even if we conclude that charge transport in the SURMOF layers is due to hopping as discussed further below.

After having checked the dependence of β on the applied voltage (Figure S11 in the Supporting Information) and having seen that it shows no significant variation, we use 0.5 V as specific value for V. This is in analogy to what is reported in the literature for SAMs in Hg-based tunneling junctions.[31] As shown in Figure 3b, the obtained attenuation factor β corresponds to ca. 0.006 $Å^{-1}$. This value is extremely low with respect to those of SAMs[25−28,31,41,42] consisting of short, purely organic molecular wires, but it is in line with what is found for "longer" organic molecular wires[42] or Hg-based tunneling junctions in which metal−organic molecular wires of a length up to 40 nm[40] were integrated. In these latter systems, low-lying energy states were provided by incorporating in the organic backbone easily oxidizable metal centers that appeared involved in a multistep charge hopping mechanism, yielding a linear increase of resistance with length (or conductance vs inverse length).[40]

As shown in the inset of Figure 3b, our data are also compatible with such a linear, ohmic increase as expected for a charge hopping mechanism. From a linear fit $RA = R_cA + \rho L$, we obtain a high resistivity ρ of 6.8×10^{12} Ω m. In the expression, R is the resistance of the whole Hg/HDT//HKUST-1/CMMT/Au system. It consists of the resistance of the SURMOF film $\rho L/A$ of thickness L and any other series resistances in the system that are summarized in the contact resistance R_c. This contact resistance will for instance contain contributions from transport through the HDT and CMMT layers. Since we vary only the thickness of the SURMOF, our statements on conduction mechanisms concern this layer, whereas R_c in other parts of the system may arise from hopping, tunneling, or mixtures.

The linear, algebraic increase in resistance with film thickness (Figure 3b) is generally not compatible with the exponential increase in resistance with thickness as expected for coherent tunneling. Attempts to fit the data with the exponential decay law $G = G_c \exp(-\beta L)$ yield β values as low as 0.006 $Å^{-1}$. This corresponds to an effective tunneling barrier φ of 0.034 meV, if we use $\beta = 2(2m_e\varphi)^{1/2}/\hbar$ with the electron mass m_e.[43] Such a vanishingly small tunneling barrier would imply good conduction due to molecular states being in resonance with the Fermi level of the Hg/HDT//HKUST-1/CMMT/Au system, an assumption which is not valid here. We thus feel that coherent tunneling does not adequately describe our data, and we conclude that the reported insulating behavior[24,38] together with our measured high resistivity suggests an off-resonant hopping transport in the HKUST-1 films.

To understand the charge-transport mechanism in the SURMOF and to explain the shallow dependence of conductance on length, we have studied a toy model that describes the transition from tunneling to hopping conduction.[33] As detailed in the Supporting Information, the SURMOF is modeled by a one-dimensional chain. The chain sites correspond to the Cu_2 centers, and the coupling of adjacent sites (only nearest neighbor couplings are considered) is via the benzene moiety of the trimesic acid linker. The model takes dephasing into account by connecting each chain site to an external, phase-randomizing reservoir. Assuming off-resonant transport, we observe a transition from a fast, exponentially decaying conductance to an inverse ohmic length dependence, consistent with the inset of Figure 3b. Over a certain interval of wire lengths, this latter ohmic regime can be well-approximated by an exponential law with a low β. On the basis of the results of these theoretical considerations, we explain the low β observed for our insulating, several tens of nanometers thick SURMOF films as being due to ohmic, incoherent hopping of charge carriers.

Porous MOFs and SURMOFs can host small molecules that can modulate and increase the conductivity of the framework.[24,38,44] In particular, the electrical transport properties of HKUST-1 films have been enhanced by inserting in the framework's pores electroactive species and small molecules, such as iodine[44] or TCNQ.[38] Such doping has led to thin films with a conductivity by far higher than those of the undoped films (about 2 orders of magnitude in the case of iodine loading[44] and 6 orders of magnitude when using TCNQ as guest molecule[38]). In both cases, the increase in electrical conductivity has been explained on the basis of the interaction between the MOF (either organic linkers[44] or inorganic dimeric nodes[38]) and the guest molecules. Additionally, ferrocene molecules have been used as guests in HKUST-1 oriented thin films[24] where, as determined on the basis of cyclic voltammetry experiments, they act as redox mediators, triggering a charge hopping transport mechanism that involves the same ferrocene molecules immobilized in the pores of the framework.

To gain further insight into the charge-transport mechanism when using ferrocene molecules as guests, we incorporated them in the HKUST-1 SURMOF pores. The loading was done according to the literature[24] and proved by IRRA spectroscopy (Figure S3 in the Supporting Information) and out-of-plane XRD. As shown in Figure 2a (red), after loading with ferrocene, a decrease in the intensity of the (222) reflex and an increase in the intensity of the (333) feature occur. The changes in the relative intensities of the (222) and (333) peaks can be attributed to changes in the structure form factor (with a partial change from a F- to an I-type lattice) associated with incorporation of ferrocene molecules in the pores of HKUST-1 (Figure 2a,b).[45] The observed shift indicates a lattice expansion and an increase in the ordering of the (111) planes, occurring as a consequence of the presence of ferrocene molecules inside the pores, with no significant change of the lattice constants (Figure S6 in the Supporting Information).

The current flowing through the Hg/HDT//HKUST-1/CMMT/Au junction, assembled as described above but with the Fc-loaded SURMOFs, was measured for the same

DOI: 10.1021/acsami.5b01792
ACS Appl. Mater. Interfaces 2015, 7, 9824−9830

thicknesses (5, 7, and 10 spraying cycles) as in the case of the pristine HKUST-1 SURMOFs. As can be seen in Figure 3a for the 5 cycles samples (and in Figure S9 in the Supporting Information for 7 and 10 spraying cycles), the J values are always larger for the Fc-loaded HKUST-1 SURMOFs than for the corresponding pristine samples. The increase for the thinnest sample is slightly larger (5.4 times) than for the thickest one (2.8 times), in line with the presented theoretical model (see the Supporting Information). Indeed, the slightly larger beta value for the Fc-loaded samples, related to a faster decay of the conductance in these samples than in the pristine SURMOFs, leads to a decrease in the conductance ratio with an increase in MOF film thickness. The measured better conductivity after the ferrocene loading suggests that the ferrocene has an effect on the electronic properties of HKUST-1. However, when plotting log$J$ vs film thickness (Figure 3b), we find a similar dependence of the current density values on the thickness as for the pristine SURMOF samples. The β value appears, within the error bars, barely modified. Nevertheless, its slight increase (0.008 $Å^{-1}$) is in agreement with the theoretical model, where an increase toward the ferrocene loaded case is proposed. As shown in the inset of Figure 3b, the data for the ferrocene-loaded SURMOFs is again compatible with a linear increase of resistance with the film thickness, but the resistivity ρ of 2.8×10^{12} Ω m is lowered by a factor of around 2.5. The results support the charge hopping regime as leading conduction mechanism also for the ferrocene-loaded HKUST-1 SURMOFs.

To further explore the changes upon Fc loading, we have performed density functional theory calculations of the pristine and Fc-loaded MOFs. We find that the ferrocene likes to bind to the benzene-based linkers through $\pi-\pi$ stacking interactions and, in terms of the electronic structure, leads to occupied states within the band gap of the MOF. We find no strongly delocalized electronic states around the band gap, as shown in the Supporting Information. The MOF states are only slightly modified due to hybridization, and molecular orbitals are either located on the ferrocene or on the MOF skeleton. For this reason no change of the charge transport mechanism is expected, as compared to the pristine framework. Although our DFT calculations cannot completely exclude that Fc molecules serve as additional hopping sites in charge transport, we rather attribute the reduction of resistance R and resistivity ρ for the ferrocene-loaded case to a better electronic coupling of the Cu_2 metal sites, possibly combined with an enhanced dephasing at these nodes. The major factors leading to the low intrinsic conductivity of HKUST-1 are the insulating behavior of the organic linkers and the bad electronic coupling of Cu_2 metallic nodes, related to the meta configuration of the benzene-derived bridges. Upon loading with ferrocene, the electronic and vibrational structures as well as the electron-vibrational couplings will be modified, as evident from the observed changes in the crystal structure (Figure 2). The enhanced effective electronic coupling and dephasing strength between and at the Cu_2 centers, leading to the improved transport properties, may stem from a partial lifting of the destructive electron interference that suppresses conduction for meta couplings.[46−48] An enhanced electron-vibration scattering due to the fluctuating interactions of the Fc molecules on top of the trimesic acid bridges at finite temperature can induce decoherence that reduces destructive interference, in addition to a purely electronic mechanism that changes left- and right-going electron paths on the benzene linker. In addition, a changed charge rearrangement at the interfaces due to the ferrocene-related states may modify the charge injection barrier.

4. CONCLUSIONS

In summary, to explore the transport properties of SURMOFs and reveal their charge transport mechanism, we have reproducibly incorporated HKUST-1 SURMOF films of different thickness in Hg-based tunneling junctions. The extremely shallow dependence of current density on film thickness, as indicated by a low value of the attenuation factor ($\beta \approx 0.006$ $Å^{-1}$), has been understood in terms of a linear, ohmic increase in resistance with length in the incoherent charge-hopping regime. The decrease in overall resistance and its weaker increase with film thickness, measured after incorporation of ferrocene inside the pores of HKUST-1 SURMOFs, indicates a reduction in the charge injection barrier and an improved electronic coupling between metal nodes.

The possibility to assemble SURMOF films in tunneling junctions paves the way toward the investigation of their transport properties and offers the possibility to gain insights into the effect of small electroactive molecules, loaded into such systems, on their electronic and transport properties. Further studies using SURMOFs of different chemical compositions or crystallographic orientation as well as different guest molecules are in progress.

■ ASSOCIATED CONTENT

Supporting Information

Infrared reflection absorption (IRRA) spectra; out-of-plane X-ray diffraction spectra; atomic force microscopy (AFM) images; investigation of the stability of HKUST-1 SURMOF under the used experimental conditions; semilog plots of voltage vs current density for 7 and 10 spraying cycles SURMOF HKUST-1, pristine and after ferrocene loading; investigation of the stability of the junction under application of a higher vertical force; length dependence of conduction; electronic structure analysis and theoretical analysis of the conduction mechanism. This material is available free of charge via the Internet at http://pubs.acs.org.

■ AUTHOR INFORMATION

Corresponding Authors

*E-mail: veronica.mugnaini@kit.edu.
*E-mail: christof.woell@kit.edu.

Author Contributions

The manuscript was written through contributions of all authors. All authors have given approval to the final version of the manuscript.

Funding

J.L. acknowledges the China Scholarship Council (CSC) for financial aid. V.M. thanks the European Union for funding (FP7-PEOPLE-2011-IEF; Project MOLSURMOF; No 301110). F.P. and A.I. thank the Carl Zeiss foundation and the Junior Professorship program of the Ministry of Science, Research, and Arts of Baden-Württemberg for support. M.Z. and T.W. thank the Deutsche Forschungsgemeinschaft for funding (Project ZH 63/14−2).

Notes

The authors declare no competing financial interest.

DOI: 10.1021/acsami.5b01792
ACS Appl. Mater. Interfaces 2015, 7, 9824−9830

REFERENCES

(1) Zhu, Q. L.; Xu, Q. Metal-Organic Framework Composites. *Chem. Soc. Rev.* **2014**, *43*, 5468−5512.
(2) Furukawa, H.; Cordova, K. E.; O'Keeffe, M.; Yaghi, O. M. The Chemistry and Applications of Metal-Organic Frameworks. *Science* **2013**, *341*, 974.
(3) Ferey, G. Hybrid Porous Solids: Past, Present, Future. *Chem. Soc. Rev.* **2008**, *37*, 191−214.
(4) Kitagawa, S.; Kitaura, R.; Noro, S. Functional Porous Coordination Polymers. *Angew. Chem., Int. Ed.* **2004**, *43*, 2334−2375.
(5) Yaghi, O. M.; O'Keeffe, M.; Ockwig, N. W.; Chae, H. K.; Eddaoudi, M.; Kim, J. Reticular Synthesis and the Design of New Materials. *Nature* **2003**, *423*, 705−714.
(6) He, Y. B.; Zhou, W.; Qian, G. D.; Chen, B. L. Methane Storage in Metal-Organic Frameworks. *Chem. Soc. Rev.* **2014**, *43*, 5657−5678.
(7) Suh, M. P.; Park, H. J.; Prasad, T. K.; Lim, D. W. Hydrogen Storage in Metal-Organic Frameworks. *Chem. Rev.* **2012**, *112*, 782−835.
(8) Makal, T. A.; Li, J. R.; Lu, W. G.; Zhou, H. C. Methane Storage in Advanced Porous Materials. *Chem. Soc. Rev.* **2012**, *41*, 7761−7779.
(9) Horcajada, P.; Gref, R.; Baati, T.; Allan, P. K.; Maurin, G.; Couvreur, P.; Ferey, G.; Morris, R. E.; Serre, C. Metal-Organic Frameworks in Biomedicine. *Chem. Rev.* **2012**, *112*, 1232−1268.
(10) Kreno, L. E.; Leong, K.; Farha, O. K.; Allendorf, M.; Van Duyne, R. P.; Hupp, J. T. Metal-Organic Framework Materials as Chemical Sensors. *Chem. Rev.* **2012**, *112*, 1105−1125.
(11) Lee, J.; Farha, O. K.; Roberts, J.; Scheidt, K. A.; Nguyen, S. T.; Hupp, J. T. Metal-Organic Framework Materials as Catalysts. *Chem. Soc. Rev.* **2009**, *38*, 1450−1459.
(12) Stavila, V.; Talin, A. A.; Allendorf, M. D. MOF-Based Electronic and Optoelectronic Devices. *Chem. Soc. Rev.* **2014**, *43*, 5994−6010.
(13) Falcaro, P.; Ricco, R.; Doherty, C. M.; Liang, K.; Hill, A. J.; Styles, M. J. MOF Positioning Technology and Device Fabrication. *Chem. Soc. Rev.* **2014**, *43*, 5513−5560.
(14) Morozan, A.; Jaouen, F. Metal Organic Frameworks for Electrochemical Applications. *Energy Environ. Sci.* **2012**, *5*, 9269−9290.
(15) D'Alessandro, D. M.; Kanga, J. R. R.; Caddy, J. S. Towards Conducting Metal-Organic Frameworks. *Aust. J. Chem.* **2011**, *64*, 718−722.
(16) Allendorf, M. D.; Schwartzberg, A.; Stavila, V.; Talin, A. A. A Roadmap to Implementing Metal-Organic Frameworks in Electronic Devices: Challenges and Critical Directions. *Chem.—Eur. J.* **2011**, *17*, 11372−11388.
(17) Zhang, Z. Y.; Yoshikawa, H.; Awaga, K. Monitoring the Solid-State Electrochemistry of Cu(2,7-AQDC) (AQDC = Anthraquinone Dicarboxylate) in a Lithium Battery: Coexistence of Metal and Ligand Redox Activities in a Metal-Organic Framework. *J. Am. Chem. Soc.* **2014**, *136*, 16112−16115.
(18) Wu, D. F.; Guo, Z. Y.; Yin, X. B.; Pang, Q. Q.; Tu, B. B.; Zhang, L. J.; Wang, Y. G.; Li, Q. W. Metal-Organic Frameworks as Cathode Materials for Li-O-2 Batteries. *Adv. Mater.* **2014**, *26*, 3258−3262.
(19) Sadakiyo, M.; Yamada, T.; Kitagawa, H. Rational Designs for Highly Proton-Conductive Metal-Organic Frameworks. *J. Am. Chem. Soc.* **2009**, *131*, 9906−9907.
(20) Liu, B.; Shioyama, H.; Jiang, H. L.; Zhang, X. B.; Xu, Q. Metal-Organic Framework (MOF) as a Template for Syntheses of Nanoporous Carbons as Electrode Materials for Supercapacitor. *Carbon* **2010**, *48*, 456−463.
(21) Chui, S. S. Y.; Lo, S. M. F.; Charmant, J. P. H.; Orpen, A. G.; Williams, I. D. A Chemically Functionalizable Nanoporous Material [Cu-3(TMA)(2)(H_2O)(3)](n). *Science* **1999**, *283*, 1148−1150.
(22) Zacher, D.; Shekhah, O.; Wöll, C.; Fischer, R. A. Thin Films of Metal-Organic Frameworks. *Chem. Soc. Rev.* **2009**, *38*, 1418−1429.
(23) Shekhah, O.; Wang, H.; Kowarik, S.; Schreiber, F.; Paulus, M.; Tolan, M.; Sternemann, C.; Evers, F.; Zacher, D.; Fischer, R. A.; Wöll, C. Step-by-Step Route for the Synthesis of Metal-Organic Frameworks. *J. Am. Chem. Soc.* **2007**, *129*, 15118−15119.
(24) Drägasser, A.; Shekhah, O.; Zybaylo, O.; Shen, C.; Buck, M.; Wöll, C.; Schlettwein, D. Redox Mediation Enabled by Immobilised Centres in the Pores of a Metal-Organic Framework Grown by Liquid Phase Epitaxy. *Chem. Commun.* **2012**, *48*, 663−665.
(25) Tran, E.; Rampi, M. A.; Whitesides, G. M. Electron Transfer in a Hg-SAM//SAM-Hg Junction Mediated by Redox Centers. *Angew. Chem., Int. Ed.* **2004**, *43*, 3835−3839.
(26) Rampi, M. A.; Whitesides, G. M. A Versatile Experimental Approach for Understanding Electron Transport through Organic Materials. *Chem. Phys.* **2002**, *281*, 373−391.
(27) Holmlin, R. E.; Ismagilov, R. F.; Haag, R.; Mujica, V.; Ratner, M. A.; Rampi, M. A.; Whitesides, G. M. Correlating Electron Transport and Molecular Structure in Organic Thin Films. *Angew. Chem., Int. Ed.* **2001**, *40*, 2316−2320.
(28) Holmlin, R. E.; Haag, R.; Chabinyc, M. L.; Ismagilov, R. F.; Cohen, A. E.; Terfort, A.; Rampi, M. A.; Whitesides, G. M. Electron Transport through Thin Organic Films in Metal-Insulator-Metal Junctions Based on Self-Assembled Monolayers. *J. Am. Chem. Soc.* **2001**, *123*, 5075−5085.
(29) Liu, J. X.; Shekhah, O.; Stammer, X.; Arslan, H. K.; Liu, B.; Schupbach, B.; Terfort, A.; Wöll, C. Deposition of Metal-Organic Frameworks by Liquid-Phase Epitaxy: The Influence of Substrate Functional Group Density on Film Orientation. *Materials* **2012**, *5*, 1581−1592.
(30) Arslan, H. K.; Shekhah, O.; Wohlgemuth, J.; Franzreb, M.; Fischer, R. A.; Wöll, C. High-Throughput Fabrication of Uniform and Homogenous MOF Coatings. *Adv. Funct. Mater.* **2011**, *21*, 4228−4231.
(31) Querebillo, C. J.; Terfort, A.; Allara, D. L.; Zharnikov, M. Static Conductance of Nitrile-Substituted Oligophenylene and Oligo-(Phenylene Ethynylene) Self-Assembled Mono Layers Studied by the Mercury-Drop Method. *J. Phys. Chem. C* **2013**, *117*, 25556−25561.
(32) Haag, R.; Rampi, M. A.; Holmlin, R. E.; Whitesides, G. M. Electrical Breakdown of Aliphatic and Aromatic Self-Assembled Monolayers Used as Nanometer-Thick Organic Dielectrics. *J. Am. Chem. Soc.* **1999**, *121*, 7895−7906.
(33) D'Amato, J. L.; Pastawski, H. M. Conductance of a Disordered Linear-Chain Including Inelastic-Scattering Events. *Phys. Rev. B* **1990**, *41*, 7411−7420.
(34) *TURBOMOLE 6.5*, TURBOMOLE GmbH Karlsruhe; http://www.turbomole.com. TURBOMOLE is a development of the University of Karlsruhe and Forschungszentrum Karlsruhe 1989−2007, TURBOMOLE GmbH since 2007.
(35) Grimme, S.; Antony, J.; Ehrlich, S.; Krieg, H. A Consistent and Accurate Ab Initio Parametrization of Density Functional Dispersion Correction (DFT-D) for the 94 Elements H-Pu. *J. Chem. Phys.* **2010**, *132*, 154104.
(36) Schäfer, A.; Huber, C.; Ahlrichs, R. Fully Optimized Contracted Gaussian-Basis Sets of Triple Zeta Valence Quality for Atoms Li to Kr. *J. Chem. Phys.* **1994**, *100*, 5829−5835.
(37) St. Petkov, P.; Vayssilov, G. N.; Liu, J. X.; Shekhah, O.; Wang, Y. M.; Wöll, C.; Heine, T. Defects in MOFs: A Thorough Characterization. *ChemPhysChem* **2012**, *13*, 2025−2029.
(38) Talin, A. A.; Centrone, A.; Ford, A. C.; Foster, M. E.; Stavila, V.; Haney, P.; Kinney, R. A.; Szalai, V.; El Gabaly, F.; Yoon, H. P.; Leonard, F.; Allendorf, M. D. Tunable Electrical Conductivity in Metal-Organic Framework Thin-Film Devices. *Science* **2014**, *343*, 66−69.
(39) Bundschuh, S.; Kraft, O.; Arslan, H. K.; Gliemann, H.; Weidler, P. G.; Wöll, C. Mechanical Properties of Metal-Organic Frameworks: An Indentation Study on Epitaxial Thin Films. *Appl. Phys. Lett.* **2012**, *101*.
(40) Tuccitto, N.; Ferri, V.; Cavazzini, M.; Quici, S.; Zhavnerko, G.; Licciardello, A.; Rampi, M. A. Highly Conductive Similar to 40-nm-Long Molecular Wires Assembled by Stepwise Incorporation of Metal Centres. *Nat. Mater.* **2009**, *8*, 41−46.
(41) Grave, C.; Tran, E.; Samori, P.; Whitesides, G. M.; Rampi, M. A. Correlating Electrical Properties and Molecular Structure of Sams Organized between Two Metal Surfaces. *Synth. Met.* **2004**, *147*, 11−18.

DOI: 10.1021/acsami.5b01792
ACS Appl. Mater. Interfaces 2015, 7, 9824−9830

(42) Luo, L. A.; Choi, S. H.; Frisbie, C. D. Probing Hopping Conduction in Conjugated Molecular Wires Connected to Metal Electrodes. *Chem. Mater.* **2011**, *23*, 631−645.
(43) Untiedt, C.; Yanson, A. I.; Grande, R.; Rubio-Bollinger, G.; Agraït, N.; Vieira, S.; van Ruitenbeek, J. M. Calibration of the Length of a Chain of Single Gold Atoms. *Phys. Rev. B* **2002**, *66*, 085418.
(44) Lee, D. Y.; Shinde, D. V.; Yoon, S. J.; Cho, K. N.; Lee, W.; Shrestha, N. K.; Han, S. H. Cu-Based Metal-Organic Frameworks for Photovoltaic Application. *J. Phys. Chem. C* **2014**, *118*, 16328−16334.
(45) Klug, H. P.; Alexander, L. E. *X-Ray Diffraction Procedures*; Wiley: New York, 1954.
(46) Mayor, M.; Weber, H. B.; Reichert, J.; Elbing, M.; von Hanisch, C.; Beckmann, D.; Fischer, M. Electric Current through a Molecular Rod−Relevance of the Position of the Anchor Groups. *Angew. Chem., Int. Ed.* **2003**, *42*, 5834−5838.
(47) Aradhya, S. V.; Meisner, J. S.; Krikorian, M.; Ahn, S.; Parameswaran, R.; Steigerwald, M. L.; Nuckolls, C.; Venkataraman, L. Dissecting Contact Mechanics from Quantum Interference in Single-Molecule Junctions of Stilbene Derivatives. *Nano Lett.* **2012**, *12*, 1643−1647.
(48) Arroyo, C. R.; Frisenda, R.; Moth-Poulsen, K.; Seldenthuis, J. S.; Bjørnholm, T.; van der Zant, H. S. J. Quantum Interference Effects at Room Temperature in OPV-Based Single-Molecule Junctions. *Nanoscale Res. Lett.* **2013**, *8*, 234.

DOI: 10.1021/acsami.5b01792
ACS Appl. Mater. Interfaces 2015, 7, 9824−9830